

MotionCFG: Boosting Motion Dynamics via Stochastic Concept Perturbation

Byungjun Kim¹ Soobin Um^{†,2} Jong Chul Ye^{†,1}

bjkim@kaist.ac.kr soobin.um@kookmin.ac.kr jong.ye@kaist.ac.kr

¹Graduate School of AI, KAIST, Daejeon 34141, Republic of Korea

²Department of AI, Kookmin University, Seoul 02707, Republic of Korea

Abstract

Despite recent advances in Text-to-Video (T2V) synthesis, generating high-fidelity and dynamic motion remains a significant challenge. Existing methods primarily rely on Classifier-Free Guidance (CFG), often with explicit negative prompts (*e.g.*, “static”, “blurry”), to suppress undesired artifacts. However, such explicit negations frequently introduce unintended semantic bias and distort object integrity — a phenomenon we define as Content-Motion Drift. To address this, we propose MotionCFG, a framework that enhances motion dynamics by contrasting a target concept with its noise-perturbed counterparts. Specifically, by injecting Gaussian noise into the concept embeddings, MotionCFG creates localized negative anchors that encapsulate a broad complementary space of sub-optimal motion variations. Unlike explicit negations, this approach facilitates implicit hard negative mining without shifting the global semantic identity, allowing for a focused refinement of temporal details. Combined with a piecewise guidance schedule that confines intervention to the early denoising steps, MotionCFG consistently improves motion dynamics across state-of-the-art T2V frameworks with negligible computational overhead and minimal compromise in visual quality. Additionally, we demonstrate that this noise-induced contrastive mechanism is effective not only for sharpening motion trajectories but also for steering complex, non-linear concepts such as precise object numerosity, which are typically difficult to modulate via standard text-based guidance. **Our project page and demo videos are available at <https://motion-cfg.vercel.app/>.**

Keywords: Text-to-Video Generation, Classifier-Free Guidance, Motion Dynamics

1 Introduction

Text-to-Video (T2V) generation has seen remarkable progress with the advent of large-scale diffusion-based generative frameworks [5, 6, 30, 29], enabling the creation of realistic videos that faithfully reflect user-intended text descriptions. A key contributor to this success is Classifier-Free Guidance (CFG) [12], which strengthens text-conditioning signals by extrapolating the score function away from an unconditional null embedding.

However, the standard CFG is inherently motion-agnostic, which improves overall text alignment while providing no mechanism to resolve ambiguity along the motion axis specifically. When training data is dominated by static or low-motion scenes [4, 27], this indiscriminate nature of CFG tends to reinforce the dominant static modes,

[†]Corresponding authors.

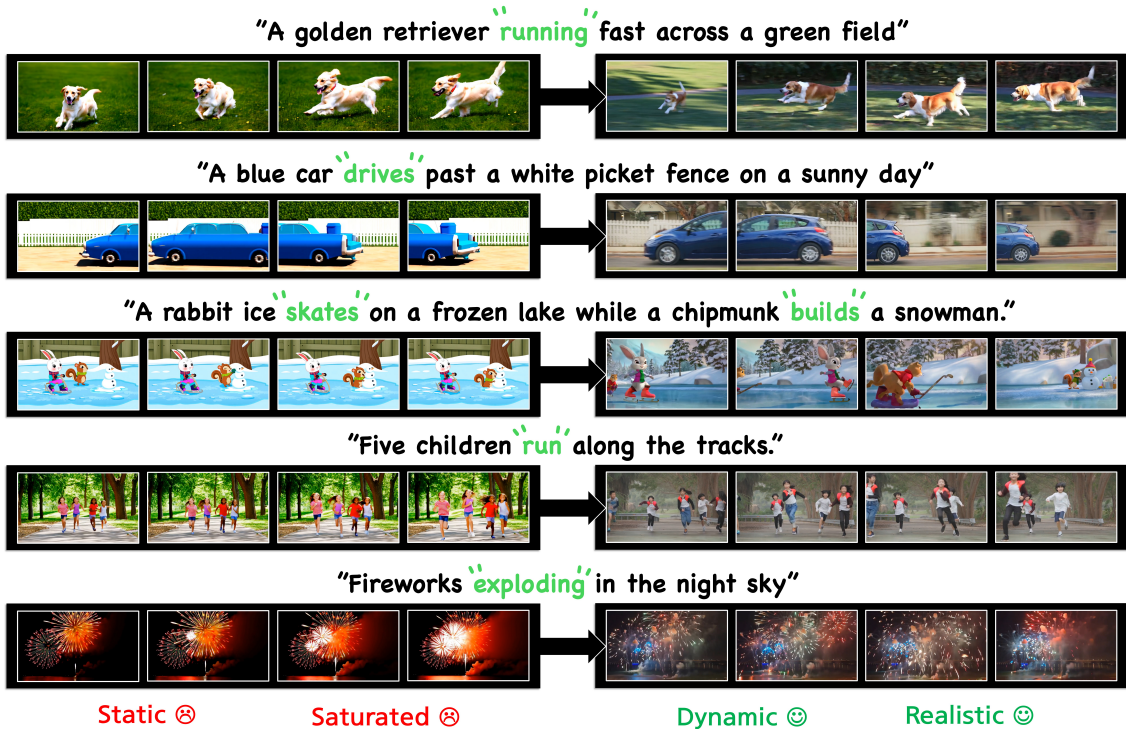


Figure 1: **Showcase of MotionCFG.** While Standard CFG (left) produces over-saturated colors and static outputs that often fail to reflect the intended actions, MotionCFG (right) resolves motion ambiguity by selectively sharpening motion-related embeddings, thereby yielding realistic and physically dynamic videos faithful to the prompt. Motion words are highlighted in green.

yielding videos with little meaningful motion even when prompted with highly dynamic actions (*e.g.*, “a cat jumping over a fence”) [22]. CFG is also known to cause over-saturation in image generation [28, 8], artifacts that similarly persist in the video domain (see Fig. 1). Classifier-Free Guidance (CFG) with explicit negative prompts (*e.g.*, “static”, “blurry”) could be used to suppress undesired artifacts. However, such explicit negations often introduce unintended semantic bias, where the structural integrity of objects is compromised while attempting to refine motion.

To address this challenge, this work proposes **MotionCFG**, a simple-yet-powerful framework designed to enhance motion dynamics in a zero-shot, training-free manner. Departing from the conventional reliance on explicit negative prompts, MotionCFG injects Gaussian noise into motion-related concept embeddings to construct localized negative anchors. Our approach begins by identifying motion-critical words, such as action verbs, within the input prompt. Drawing inspiration from manifold-constrained CFG (CFG++) [8], we then steer the T2V sampling process by following the gradient of a loss function that repels the generation away from motion-ambiguous predictions. To optimize the trade-off between dynamic intensity and visual fidelity, we introduce a Piecewise Guidance Scheduler. This scheduler strategically restricts our intervention to the initial sampling stages, where the global motion layout is established, thereby preserving fine-grained structural details in the later steps. This approach offers three distinct advantages:

- **Semantic Precision:** It suppresses a broad “complementary space” of sub-optimal

motion variations surrounding the target concept rather than avoiding a single, narrow semantic point.

- **Content Preservation:** It isolates the degradation to the motion manifold, allowing the model to sharpen dynamics without distorting the global semantic identity of the objects.
- **Implicit Hard Negative Mining:** By contrasting the clean embedding with a similar but degraded noisy version, MotionCFG facilitates a more rigorous refinement of fine-grained temporal details without the need for manual negative prompt engineering.

We validate MotionCFG on state-of-the-art T2V models including Wan2.1 [29] (1.3B and 14B) and CogVideoX [30], demonstrating consistent improvements in motion dynamics with marginal compromise in text-video alignment across diverse prompts, all with negligible computational overhead over the standard CFG sampler. Beyond enhancing motion dynamics, we further demonstrate the versatility of our approach by successfully addressing other notoriously difficult-to-control concepts, such as precise object counting. Our results suggest that the noise-induced contrastive mechanism serves as a generalized framework for steering discrete or non-linear semantic attributes that remain elusive to standard text-based guidance, establishing MotionCFG as a robust tool for high-fidelity, controllable concept synthesis.

2 Related Work

Text-to-Video Generation. Text-to-Video (T2V) generation has evolved rapidly, transitioning from 3D-UNet based diffusion models [13, 25] to Flow-Matching (FM) frameworks [19] utilizing Diffusion Transformers (DiT). State-of-the-art open-source models like CogVideoX [30] and WAN [29] leverage large-scale datasets and 3D causal VAEs to achieve high spatiotemporal consistency. Despite their impressive visual quality, these models heavily rely on standard cross-attention mechanisms for text conditioning, which often fail to parse fine-grained physical dynamics, leading to the aforementioned mode averaging in complex motion generation.

Motion Dynamics in Video Generation. Current text-to-video (T2V) models frequently suffer from a static bias, where generated outputs exhibit minimal temporal variation or resemble static images with subtle camera drift. This limitation is primarily attributed to the characteristics of large-scale training datasets, such as WebVid-10M [3], which contain a high proportion of videos with limited object motion. Consequently, models often learn a shortcut toward the dominant static modes, failing to capture complex physical dynamics.

To address this, DEMO [22] proposes a framework that decomposes text encoding and conditioning into distinct content and motion components. While effective at enhancing motion synthesis from textual descriptions, DEMO necessitates a specialized and computationally expensive training process involving novel text-motion and video-motion supervision losses. In the image-to-video (I2V) domain, ALG [7] identifies that motion suppression often stems from premature exposure to high-frequency signals in the conditioning image, which biases the sampling process toward a static appearance. While ALG provides a training-free solution by adaptively modulating the reference image’s frequency content, its application is fundamentally restricted to models that incorporate an external visual condition.

In contrast, our MotionCFG addresses motion dynamics within general T2V frameworks in a training-free manner. Unlike DEMO, MotionCFG requires no architectural modifications or specialized supervision. Furthermore, while sharing the inference-time efficiency of ALG, MotionCFG extends motion enhancement beyond the constraints of I2V conditioning by operating directly on the semantic embedding space of the text prompt. **Guidance Mechanisms in Diffusion Models.** Classifier-Free Guidance (CFG) is the de facto standard for aligning diffusion outputs with text prompts [12]. While effective for static attributes, it struggles with motion ambiguity since extrapolating away from an empty string (\emptyset) does not inherently resolve the specific dynamic intent. Recent works have explored explicit negative prompt, gradient-based guidance or attention-map manipulations. CFG++ [8] reformulates the guidance as a manifold-constrained optimization via score distillation, improving sample quality by anchoring updates on the clean data manifold. Our theoretical analysis builds on this framework but extends it to a dual-condition setting, where the repulsion target is a motion-perturbed prediction rather than an unconditional one or an explicit negative concept.

3 Method

3.1 Preliminaries

Text-to-Video Diffusion Models. Modern diffusion-based text-to-video (T2V) models [5, 6, 30, 29] operate in the latent space of a 3D variational autoencoder (VAE) [15], which consists of an encoder $E(\cdot)$ and a decoder $D(\cdot)$. A video \mathbf{x} is first compressed into a low-dimensional latent representation $\mathbf{z}_0 = E(\mathbf{x})$. The diffusion forward process gradually corrupts \mathbf{z}_0 by adding Gaussian noise according to a variance schedule, producing a noisy latent \mathbf{z}_t at timestep t [11]. A neural network is then trained to reverse this corruption by learning to predict the added noise $\epsilon_\theta(\mathbf{z}_t, \mathbf{c})$ [11], where \mathbf{c} denotes the text condition embedded by a pretrained text encoder (*e.g.*, T5 [21]). Generation proceeds by iteratively denoising from pure noise $\mathbf{z}_T \sim \mathcal{N}(\mathbf{0}, \mathbf{I})$ back to a clean latent \mathbf{z}_0 using the learned noise predictor, which is then decoded to pixel space via $\hat{\mathbf{x}} = D(\mathbf{z}_0)$.

Classifier-Free Guidance. Classifier-Free Guidance (CFG) [12] improves text-conditional generation by extrapolating between the unconditional and conditional noise predictions:

$$\tilde{\epsilon}_\theta(\mathbf{z}_t, \mathbf{c}, \emptyset) = \epsilon_\theta(\mathbf{z}_t, \emptyset) + \omega_{\text{std}} (\epsilon_\theta(\mathbf{z}_t, \mathbf{c}) - \epsilon_\theta(\mathbf{z}_t, \emptyset)), \quad (1)$$

where \emptyset denotes the null (unconditional) embedding and $\omega_{\text{std}} > 1$ is the guidance scale. By extrapolating the noise prediction away from the unconditional estimate, CFG sharpens the conditional distribution and strengthens text alignment. However, this *extrapolation* operates on the *entire* condition vector \mathbf{c} uniformly, offering no mechanism to selectively resolve ambiguity in specific semantic dimensions such as motion. In practice, video training datasets are heavily skewed toward static or low-motion scenes [4, 27], and CFG’s uniform operation tends to reinforce these dominant modes, yielding videos with little meaningful motion even for highly dynamic prompts [22].

A natural remedy is *negative prompting* [9]: replacing the null embedding in Eq. (1) with a text condition that explicitly describes static or low-motion scenes (*e.g.*, “static, still picture”), thereby steering the generation away from stillness. In practice, however, this coarse textual intervention yields only marginal gains over standard null-prompted CFG (see Table 3), as a single hand-crafted sentence may not capture the fine-grained motion semantics encoded across individual tokens. This motivates a more principled approach that operates directly in the embedding space rather than at the text level.

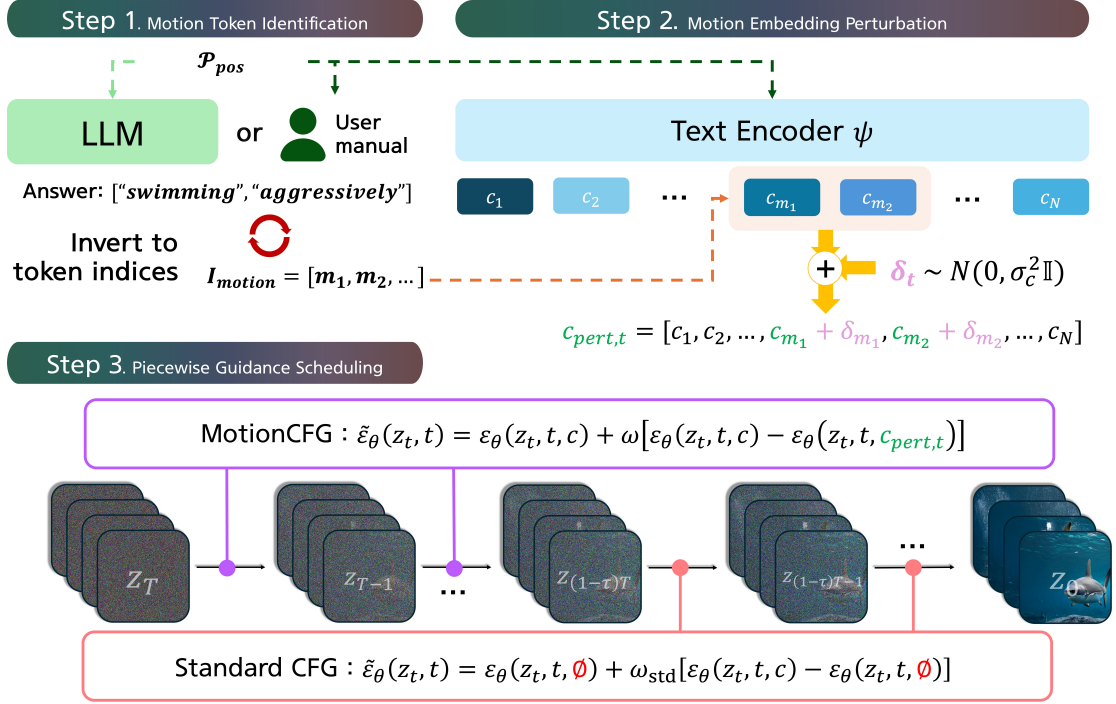


Figure 2: **Overview of the MotionCFG pipeline.** **Step 1:** Motion-related tokens in the prompt are identified via an LLM. **Step 2:** Gaussian noise (δ_t) is injected exclusively into these motion text embeddings to generate a perturbed condition ($c_{pert,t}$). **Step 3:** A piecewise guidance schedule applies MotionCFG during the early sampling steps to establish robust motion trajectories, before reverting to standard CFG to refine spatial details.

3.2 MotionCFG

We introduce MotionCFG, a training-free sampler that rectifies the inherent low-motion bias of T2V models by replacing conventional null embeddings or hand-crafted negative prompts with motion-perturbed negative anchors. This strategic refinement ensures semantic precision by repelling the generation away from a *distribution of localized hard negatives*, representing a continuous neighborhood of degraded and sub-optimal motion variations surrounding the target concept. By localizing perturbations to the motion manifold, MotionCFG facilitates content preservation, sharpening dynamic trajectories without the *Content-Motion Drift*, which is typical in explicit negations. Furthermore, this noise-injected formulation enables implicit hard negative mining, forcing the model to discern fine-grained temporal details from their degraded counterparts.

Specifically, given an input text prompt, let $\mathbf{c} \in \mathbb{R}^{L \times d}$ denote its embedding sequence obtained from the pretrained text encoder, where L is the sequence length and d is the embedding dimension. We first identify a set of motion-related tokenized indices $\mathcal{I}_{\text{motion}}$ (e.g., action verbs such as “jumping” or “running”). At each denoising step t , we sample a fresh noise vector $\mathbf{n}_t \sim \mathcal{N}(\mathbf{0}, \mathbf{I})$ and construct a perturbed embedding $\mathbf{c}_{\text{pert},t}$ by injecting noise exclusively into the text embeddings at the identified indices:

$$\mathbf{c}_{\text{pert},t}[i] = \begin{cases} \mathbf{c}[i] + \sigma_c \mathbf{n}_t, & \text{if } i \in \mathcal{I}_{\text{motion}} \\ \mathbf{c}[i], & \text{otherwise} \end{cases} \quad (2)$$

where $\sigma_c > 0$ controls the perturbation magnitude. The guided noise prediction is then

computed by steering generation away from this perturbed neighborhood:

$$\tilde{\epsilon}_\theta(\mathbf{z}_t, \mathbf{c}, \mathbf{c}_{\text{pert},t}) = \epsilon_\theta(\mathbf{z}_t, \mathbf{c}_{\text{pert},t}) + \omega (\epsilon_\theta(\mathbf{z}_t, \mathbf{c}) - \epsilon_\theta(\mathbf{z}_t, \mathbf{c}_{\text{pert},t})), \quad (3)$$

where \mathbf{c} and $\mathbf{c}_{\text{pert},t}$ denote the conditions derived from the original and perturbed embeddings, respectively. Note that the anchor point is different from standard CFG in Eq. (1). Intuitively, while standard CFG extrapolates between the *unconditional* and conditional noise predictions to strengthen overall text alignment, MotionCFG steers away from a *motion-degraded* condition, thereby selectively sharpening the motion semantics without affecting the remaining attributes. A rigorous derivation of Eq. (3) will be proved later.

Piecewise Guidance Scheduling. In video diffusion models, the global motion layout is established during the earliest denoising steps, while later steps refine high-frequency spatial details and textures [2, 14]. Applying Eq. (3) throughout the entire sampling process introduces unnecessary stochastic variance in the late stage, often resulting in visual artifacts. We therefore introduce a piecewise schedule controlled by a ratio $\tau \in [0, 1]$: MotionCFG is applied during the first τ fraction of the total steps to establish the motion trajectory, after which we revert to standard CFG (Eq. (1)) for spatial refinement. To jointly improve text alignment during the motion-encouraging stage, we anchor the baseline on \mathbf{c} rather than $\mathbf{c}_{\text{pert},t}$:

$$\tilde{\epsilon}_\theta^*(\mathbf{z}_t, \mathbf{c}, \mathbf{c}_{\text{pert},t}) = \epsilon_\theta(\mathbf{z}_t, \mathbf{c}) + \omega (\epsilon_\theta(\mathbf{z}_t, \mathbf{c}) - \epsilon_\theta(\mathbf{z}_t, \mathbf{c}_{\text{pert},t})). \quad (4)$$

This two-stage approach with the \mathbf{c} -anchored formulation consistently outperforms the full-schedule variant ($\tau = 1.0$); see Fig. 4 for details. The full procedure is summarized in Algorithm 1, and an overview of the pipeline is illustrated in Fig. 2.

Motion Token Identification. Identifying $\mathcal{I}_{\text{motion}}$ requires determining which parts of the text embeddings in the prompt carry motion semantics. Users can manually specify target verbs for best precision, but this becomes tedious when processing large prompt sets. To sidestep this, we automate the identification by querying a lightweight large language model (*e.g.*, Qwen2.5-7B-Instruct) via in-context learning. Specifically, we feed the prompt with its tokenized indices (*e.g.*, [0]A [1]cat [2]jumps) and instruct the model to return the indices of words describing physical actions or dynamic changes. Importantly, the computational overhead introduced by this automated extraction is marginal compared to the overall video diffusion process. Detailed complexity analysis, along with the instruction template, is provided in the supplementary.

3.3 Motion-Aware Guidance as Manifold-Constrained Extrapolation

Here we explore a theoretical intuition behind the MotionCFG guidance. In particular, we show that the guided noise prediction in Eq. (3) can be reformulated as a manifold-constrained optimization problem inspired by CFG++ [8], where the update extrapolates along the clean data manifold away from a motion-ambiguous prediction.

Given the noisy latent \mathbf{z}_t , we formulate the Tweedie estimates for the target appearance (\mathbf{c}) and perturbed ($\mathbf{c}_{\text{pert},t}$) manifolds directly using the noise prediction network ϵ_θ :

$$\hat{\mathbf{z}}_{\mathbf{c}} := \frac{1}{\sqrt{\bar{\alpha}_t}} (\mathbf{z}_t - \sqrt{1 - \bar{\alpha}_t} \epsilon_\theta(\mathbf{z}_t, \mathbf{c})), \quad (5)$$

$$\hat{\mathbf{z}}_{\text{pert}} := \frac{1}{\sqrt{\bar{\alpha}_t}} (\mathbf{z}_t - \sqrt{1 - \bar{\alpha}_t} \epsilon_\theta(\mathbf{z}_t, \mathbf{c}_{\text{pert},t})), \quad (6)$$

Algorithm 1 MotionCFG Sampling

```
1: Input: User prompt  $\mathcal{P}$ , negative prompt  $\mathcal{P}_{\text{neg}}$ , model  $\epsilon_\theta$ , decoder  $\mathcal{D}$ , steps  $T$ , ratio
    $\tau \in [0, 1]$ , guidance scales  $\omega, \omega_{\text{std}}$ 
2:  $\mathcal{I}_{\text{motion}} \leftarrow \text{MotionExtract}(\mathcal{P})$  ▷ Token identification
3:  $\mathbf{c} \leftarrow \text{Encode}(\mathcal{P})$ 
4:  $\mathbf{c}_{\text{neg}} \leftarrow \text{Encode}(\mathcal{P}_{\text{neg}})$  ▷ Standard CFG negative condition
5:  $\mathbf{z}_T \sim \mathcal{N}(\mathbf{0}, \mathbf{I})$ 
6: for  $t = T \dots 1$  do
7:   if  $t > (1 - \tau)T$  then ▷ Early trajectory phase (MotionCFG)
8:      $\mathbf{n}_t \sim \mathcal{N}(\mathbf{0}, \mathbf{I})$ 
9:      $\mathbf{c}_{\text{pert},t} \leftarrow \text{Perturb}(\mathbf{c}, \mathcal{I}_{\text{motion}}, \sigma_{\mathbf{c}} \mathbf{n}_t)$  ▷ Apply Eq. (2)
10:     $\tilde{\epsilon} \leftarrow \epsilon_\theta(\mathbf{z}_t, \mathbf{c}) + \omega (\epsilon_\theta(\mathbf{z}_t, \mathbf{c}) - \epsilon_\theta(\mathbf{z}_t, \mathbf{c}_{\text{pert},t}))$  ▷ Eq. (4)
11:  else ▷ Refinement phase (Standard CFG)
12:     $\tilde{\epsilon} \leftarrow \epsilon_\theta(\mathbf{z}_t, \emptyset) + \omega_{\text{std}} (\epsilon_\theta(\mathbf{z}_t, \mathbf{c}) - \epsilon_\theta(\mathbf{z}_t, \emptyset))$  ▷ Eq. (1)
13:  end if
14:   $\mathbf{z}_{t-1} \leftarrow \text{SchedulerStep}(\mathbf{z}_t, \tilde{\epsilon})$ 
15: end for
16: Return  $\hat{\mathbf{x}} \leftarrow \mathcal{D}(\mathbf{z}_0)$ 
```

where $\bar{\alpha}_t$ denotes the cumulative noise schedule at timestep t [11]. Rather than navigating an unconstrained space, we define our guidance objective directly on $\hat{\mathbf{z}}_{\mathbf{c}}$. To resolve motion ambiguity, we aim to push this state away from the perturbed manifold $\hat{\mathbf{z}}_{\text{pert}}$. Utilizing the Score Distillation Sampling (SDS) formulation [8], we can express this repulsion by minimizing the negative SDS loss associated with the perturbed condition. We define this objective initially as the negative Mean Squared Error (MSE) between the noise predictions, which elegantly translates into the scaled squared distance between the manifold projections:

$$\begin{aligned} \mathcal{L}_M(\hat{\mathbf{z}}_{\mathbf{c}}) &:= - \left\| \epsilon_\theta(\mathbf{z}_t, \mathbf{c}) - \epsilon_\theta(\mathbf{z}_t, \mathbf{c}_{\text{pert},t}) \right\|_2^2 \\ &= - \frac{\bar{\alpha}_t}{1 - \bar{\alpha}_t} \left\| \hat{\mathbf{z}}_{\mathbf{c}} - \hat{\mathbf{z}}_{\text{pert}} \right\|_2^2. \end{aligned} \quad (7)$$

Minimizing Eq. (7) effectively repels the generation trajectory from the motion-ambiguous manifold $\hat{\mathbf{z}}_{\text{pert}}$ while remaining anchored at $\hat{\mathbf{z}}_{\mathbf{c}}$. Evaluating the gradient of this objective with respect to $\hat{\mathbf{z}}_{\mathbf{c}}$ yields:

$$\nabla_{\hat{\mathbf{z}}_{\mathbf{c}}} \mathcal{L}_M(\hat{\mathbf{z}}_{\mathbf{c}}) = - \frac{2\bar{\alpha}_t}{1 - \bar{\alpha}_t} (\hat{\mathbf{z}}_{\mathbf{c}} - \hat{\mathbf{z}}_{\text{pert}}). \quad (8)$$

Stepping in the negative gradient direction with step size $\gamma_t > 0$ gives the updated manifold point:

$$\hat{\mathbf{z}}_{\text{updated}} = \hat{\mathbf{z}}_{\mathbf{c}} - \gamma_t \nabla_{\hat{\mathbf{z}}_{\mathbf{c}}} \mathcal{L}_M(\hat{\mathbf{z}}_{\mathbf{c}}) = \hat{\mathbf{z}}_{\mathbf{c}} + \frac{2\gamma_t \bar{\alpha}_t}{1 - \bar{\alpha}_t} (\hat{\mathbf{z}}_{\mathbf{c}} - \hat{\mathbf{z}}_{\text{pert}}), \quad (9)$$

which represents a *manifold-constrained extrapolation* away from ambiguity. By substituting $\hat{\mathbf{z}}_{\text{updated}}$ into the inverse Tweedie relation, $\tilde{\epsilon} = \frac{\mathbf{z}_t - \sqrt{\bar{\alpha}_t} \hat{\mathbf{z}}_{\text{updated}}}{\sqrt{1 - \bar{\alpha}_t}}$, we obtain the effective guided noise prediction:

$$\tilde{\epsilon} = \epsilon_\theta(\mathbf{z}_t, \mathbf{c}) + \frac{2\gamma_t \bar{\alpha}_t}{1 - \bar{\alpha}_t} (\epsilon_\theta(\mathbf{z}_t, \mathbf{c}) - \epsilon_\theta(\mathbf{z}_t, \mathbf{c}_{\text{pert},t})). \quad (10)$$

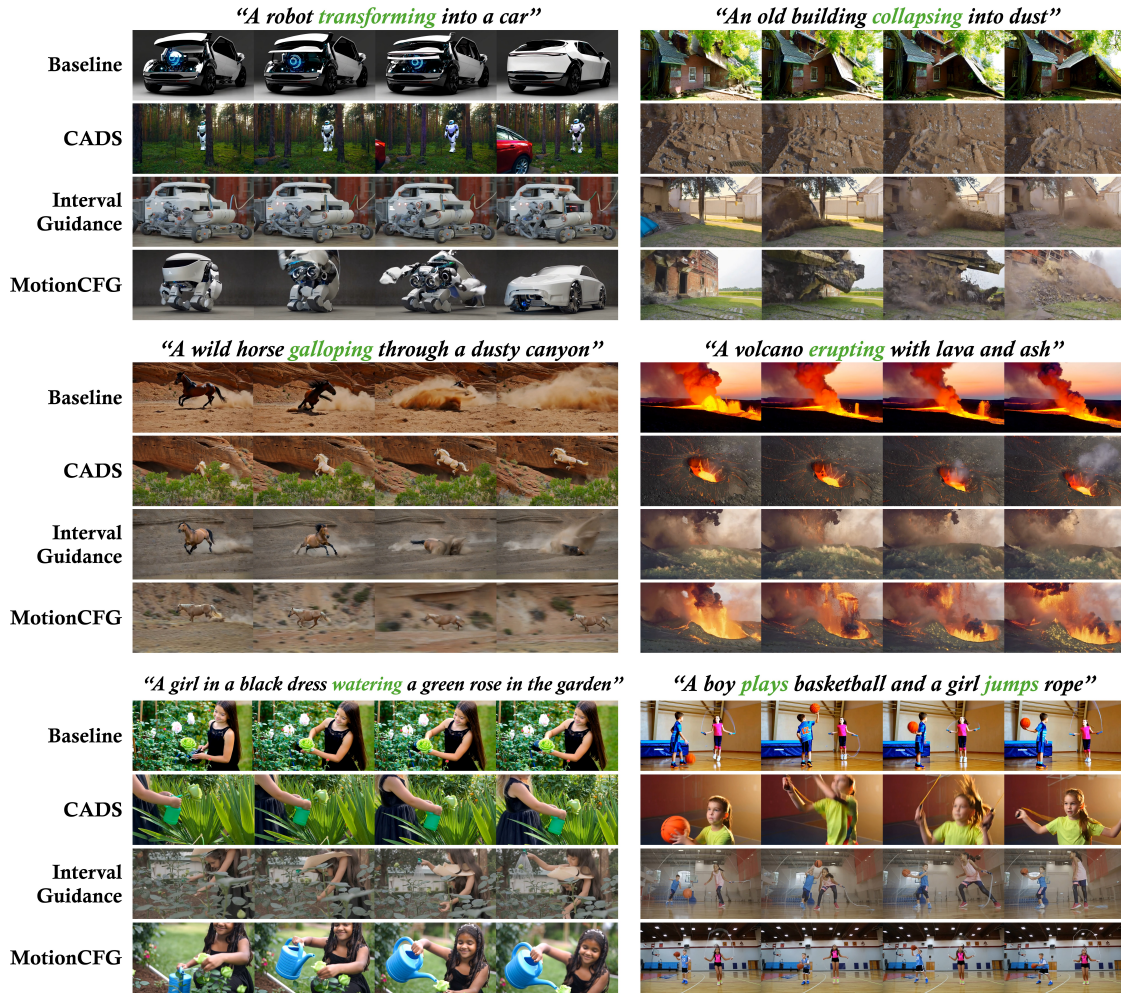


Figure 3: **Qualitative comparison on Wan2.1.** Each row shows uniformly sampled frames from a generated video. “Baseline” denotes negative-prompted CFG. While existing approaches produce near-static outputs or visual artifacts, MotionCFG generates physically plausible dynamics faithful to the highlighted motion tokens (green).

Identifying the guidance scale $\omega := \frac{2\gamma_t \bar{\alpha}_t}{1 - \bar{\alpha}_t}$, Eq. (10) exactly recovers the MotionCFG guided noise update:

$$\tilde{\epsilon} \leftarrow \epsilon_{\theta}(\mathbf{z}_t, \mathbf{c}) + \omega (\epsilon_{\theta}(\mathbf{z}_t, \mathbf{c}) - \epsilon_{\theta}(\mathbf{z}_t, \mathbf{c}_{\text{pert},t})). \quad (11)$$

This establishes that MotionCFG corresponds to the rigorous repelling from stochastic concept perturbation, where the guidance scale ω explicitly controls the extrapolation magnitude to sharpen dynamic semantics without corrupting the target appearance.

4 Experiments

Models and Datasets. To verify the robustness of our approach across various model scales, we conduct experiments on several state-of-the-art T2V frameworks, including Wan2.1-T2V (1.3B and 14B) and CogVideoX-5B. For quantitative and qualitative evaluation, we utilize the T2V-Compbench [26] dataset. However, as T2V-Compbench does not explicitly prioritize or categorize high-magnitude motion dynamics, we curate an additional set of motion-intensive prompts using Gemini to specifically assess dynamic fidelity.

Table 1: **Quantitative comparison on Gemini-generated prompts.** “Baseline” denotes negative-prompted CFG. MotionCFG (Ours) consistently demonstrates superior performance in temporal dynamics across various base models. Upward arrows (\uparrow) indicate higher is better, while downward arrows (\downarrow) indicate lower is better.

Model	Method	Frame-wise		Full Video	Dynamics / Temporal				
		CLIPScore \uparrow	PickScore \uparrow	X-CLIP \uparrow	SSIM \downarrow	FLOW \uparrow	Info DINO \uparrow	DINO Segm. \uparrow	DEVIL \uparrow
Wan2.1-1.3B	Baseline	0.2535	0.2092	22.2128	0.7193	4.0962	0.0555	0.3842	0.3069
	CADS	0.2496	0.2104	22.7687	0.6476	2.2151	0.0294	0.3553	0.1973
	IG	0.2392	0.2058	23.0677	0.7116	3.7564	0.0635	0.4420	0.3147
	Ours	0.2488	0.2089	23.3881	0.6547	4.7320	0.0650	0.4586	0.3374
Wan2.1-14B	Baseline	0.2651	0.2136	21.7438	0.8398	2.9466	0.0430	0.2853	0.2324
	CADS	0.2516	0.2112	22.1356	0.7735	2.4108	0.0467	0.3554	0.2410
	IG	0.2518	0.2112	23.0622	0.8207	2.6495	0.0571	0.3931	0.2732
	Ours	0.2519	0.2098	22.7080	0.7901	6.0557	0.0772	0.4293	0.3304
CogVideoX-5B	Baseline	0.2627	0.2140	23.4035	0.8243	2.6547	0.0384	0.3109	0.2415
	CADS	0.2534	0.2116	22.7322	0.7651	2.9304	0.0494	0.4470	0.2884
	IG	0.2539	0.2105	22.6066	0.7665	2.9594	0.0512	0.4368	0.2955
	Ours	0.2550	0.2115	22.7820	0.7666	2.9415	0.0522	0.4360	0.2976

A comprehensive description of these curated prompts and their categories is provided in the supplementary.

Baselines. We compare MotionCFG against several training-free sampling strategies. *Baseline* indicates *Negative Prompting* that replaces the null embedding in standard CFG with a text condition describing static scenes (*e.g.*, “static, still picture”); details on prompt selection are provided in the supplementary. *CADS* [23] and *Interval Guidance* [17] are state-of-the-art diversity-enhancing samplers originally proposed for text-to-image generation.

Evaluation Metrics. To comprehensively evaluate the generated videos, we employ a diverse set of metrics focusing on two main aspects: *visual quality with semantic alignment*, and *motion dynamics*. For visual quality and semantic alignment, we evaluate videos at both the frame and video levels. For frame-wise evaluation, we extract individual frames from the generated video, independently calculate **CLIPScore** [10] and **PickScore** [16], and report the averaged scores for each video. To assess the global spatio-temporal alignment between the text prompt and the entire video sequence, we employ **X-CLIP** [20], a dedicated video-language understanding metric.

To quantitatively evaluate the magnitude, complexity, and temporal dynamics of the generated motions, we adopt the evaluation protocol proposed in the **DEVIL** benchmark [18]. Specifically, we report **FLOW** (average pixel-level motion) and semantic variations using **Info DINO** and **DINO Segm.** We also report the unified **DEVIL Score**. Notably, this score is derived via regression after measuring a broader, comprehensive set of multiple dynamic indicators to provide a holistic assessment. Additionally, we employ **SSIM** to measure structural variation across adjacent frames, where a lower score indicates higher dynamic changes.

4.1 Main Results

Qualitative Evaluation. Fig. 3 compares generated videos of MotionCFG against the baselines. Standard CFG with negative prompting (“Baseline”) often produces nearly static frames, while CADS and Interval Guidance introduce artifacts such as over-saturation or subject morphing. In contrast, MotionCFG generates vigorous motion trajectories, such as the structural collapse of the building and the galloping motion of the horse, while preserving subject consistency and visual fidelity. Since static frames cannot fully

Table 2: **Quantitative comparison on T2V-CompBench.** “Baseline” indicates negative-prompted CFG. We observe that MotionCFG significantly improves temporal consistency and motion dynamics compared to existing guidance techniques. Upward arrows (\uparrow) indicate higher is better, while downward arrows (\downarrow) indicate lower is better.

Model	Method	Framewise		Full Video	Dynamics / Temporal				
		CLIPScore \uparrow	PickScore \uparrow	X-CLIP \uparrow	SSIM \downarrow	FLOW \uparrow	Info DINO \uparrow	DINO Segm. \uparrow	DEVIL \uparrow
Wan2.1-1.3B	Baseline	0.2651	0.2108	22.7719	0.7720	3.0671	0.0463	0.3517	0.2528
	CADS	0.2654	0.2127	24.1668	0.7018	1.7996	0.0348	0.3536	0.2022
	IG	0.2552	0.2090	23.9607	0.6785	4.1116	0.0601	0.4761	0.3077
	Ours	0.2550	0.2085	23.7080	0.6378	6.5136	0.0726	0.5034	0.3531
Wan2.1-14B	Baseline	0.2755	0.2147	23.1646	0.8770	1.7147	0.0378	0.2561	0.1995
	CADS	0.2630	0.2121	23.1093	0.7853	3.5325	0.0438	0.3464	0.2286
	IG	0.2579	0.2092	23.2270	0.8223	1.7266	0.0571	0.3893	0.2581
	Ours	0.2593	0.2097	23.0819	0.8025	4.4839	0.0727	0.4213	0.3057

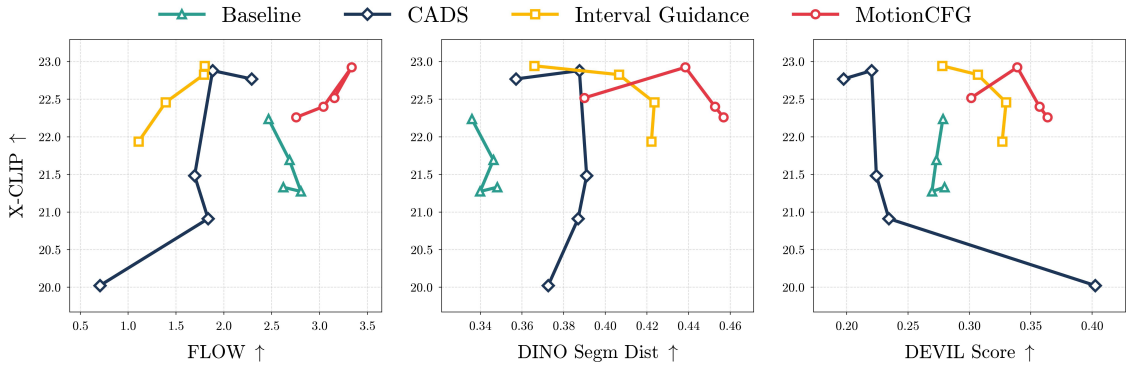


Figure 4: **Trade-off analysis between text fidelity and motion dynamics.** Each point corresponds to a different hyperparameter choice (*e.g.*, ratio τ). MotionCFG (red) achieves higher motion scores (FLOW, Dino Segm Dist, DEVIL) with minimal X-CLIP degradation, while baselines either sacrifice fidelity or fail to improve dynamics.

convey these temporal improvements, we provide high-resolution video comparisons in the supplementary.

Quantitative Results. Tables 1 and 2 present quantitative comparisons across all base models and prompt sets. MotionCFG consistently achieves high scores in FLOW, DINO Segm., and DEVIL, confirming its effectiveness in enhancing temporal dynamics at multiple granularities. Notably, on Wan2.1-14B, MotionCFG more than doubles the FLOW score of the baseline (6.06 vs. 2.95) while maintaining comparable X-CLIP. CADS tends to suppress motion (lower FLOW than baseline in most settings), and Interval Guidance offers moderate gains but at the cost of reduced CLIPScore. In contrast, MotionCFG amplifies motion dynamics with only marginal trade-offs in frame-wise fidelity metrics, demonstrating a favorable balance between dynamics and visual quality.

Trade-off Analysis. Fig. 4 visualizes the text fidelity–motion dynamics trade-off by sweeping each method’s hyperparameters. MotionCFG occupies the upper-right region across all three dynamics metrics, achieving stronger motion with minimal X-CLIP degradation. Baseline and Interval Guidance cluster in a narrow range, indicating limited controllability over dynamics. CADS can reach high FLOW and DINO Segm Dist values, but only at a severe X-CLIP cost; its curve drops steeply as dynamics increase. In contrast, MotionCFG’s Pareto frontier remains nearly flat, demonstrating that motion intensity can be scaled without sacrificing semantic fidelity.

Table 3: **Ablation on perturbation target.** We vary which embedding regions are perturbed: none (Null-Prompted), all via negative text (Neg-Prompted), non-motion tokens ($\mathcal{I}_{\text{motion}}^c$), and motion tokens via LLM or manual selection. Perturbing motion tokens yields the strongest dynamics with minimal X-CLIP degradation.

Method	X-CLIP \uparrow	Info DINO \uparrow	DINO Segm. \uparrow	DEVIL Score \uparrow
Null-Prompted	22.2696	0.0597	0.3594	0.3083
Neg-Prompted	22.2128	0.0555	0.3842	0.3069
Non-motion perturbed ($\mathcal{I}_{\text{motion}}^c$)	21.9169	0.0805	0.4208	0.3320
Motion perturbed (LLM)	22.2435	0.0929	0.4528	0.3637
Motion perturbed (Manual)	22.0997	0.0925	0.4572	0.3682

4.2 Ablation Studies

Impact of Perturbation Target and Methods. Table 3 isolates the effect of which tokens are perturbed. Null- and negative-prompted baselines show limited dynamics, confirming that standard CFG cannot resolve motion ambiguity. Perturbing embeddings of non-motion words ($\mathcal{I}_{\text{motion}}^c$) does improve dynamics, but at a disproportionate cost to text alignment, where X-CLIP drops by 0.35. This indicates that perturbing tokens unrelated to motion disrupts static semantics, such as scene layout or object identity, without providing a useful contrastive signal for dynamics. In contrast, targeting motion-related embeddings yields the strongest improvements across all metrics, with DEVIL reaching 0.37 compared to the 0.31 baseline, while keeping X-CLIP within 0.1 of the unperturbed baseline.

The LLM-based and manual identification perform comparably, confirming that our automated pipeline introduces negligible degradation.

Effect of Perturbation Strength. We analyze the impact of the perturbation scale, denoted as σ_c , on the resulting motion dynamics. As summarized in Table 4, increasing σ_c significantly enhances the magnitude of generated motions, as indicated by the rise in FLOW and DEVIL Score. While higher σ_c values introduce stronger perturbations to the motion-related embeddings, the X-CLIP score remains remarkably stable. This suggests that σ_c serves as a reliable hyperparameter for scaling motion intensity while preserving the core semantic integrity.

Effect of Guidance Schedule (τ). We investigate the influence of the guidance schedule, controlled by the timestep ratio τ , which determines the interval over which the semantic perturbation is applied. As shown in Table 5, increasing τ from 0.05 to 0.20 notably enhances high-level semantic dynamics, improving the DEVIL Score from 0.2779 to 0.3300 and DINO Segm. from 0.3660 to 0.4236. However, extending the perturba-

Table 4: **Effect of σ_c (fixed $\tau = 0.1$).** Increasing the scale provides scalable control over motion intensity.

σ_c	X-CLIP \uparrow	FLOW \uparrow	DEVIL \uparrow
0.01	23.0244	4.0177	0.3165
0.03	22.8113	4.7649	0.3291
0.05	23.3881	4.7320	0.3374
0.10	22.6914	6.3951	0.3729

Table 5: **Effect of Guidance Schedule (τ).** We vary the guidance interval τ (with fixed $w = 6.0$). While moderate intervals improve dynamics, excessive τ degrades both fidelity and motion.

τ	X-CLIP \uparrow	FLOW \uparrow	DINO Segm. \uparrow	DEVIL \uparrow
0.05	22.9430	1.8005	0.3660	0.2779
0.10	22.8258	1.7918	0.4066	0.3069
0.20	22.4572	1.3929	0.4236	0.3300
0.30	21.9369	1.1102	0.4222	0.3268

Prompt: “*Three horses gallop across the beach.*”

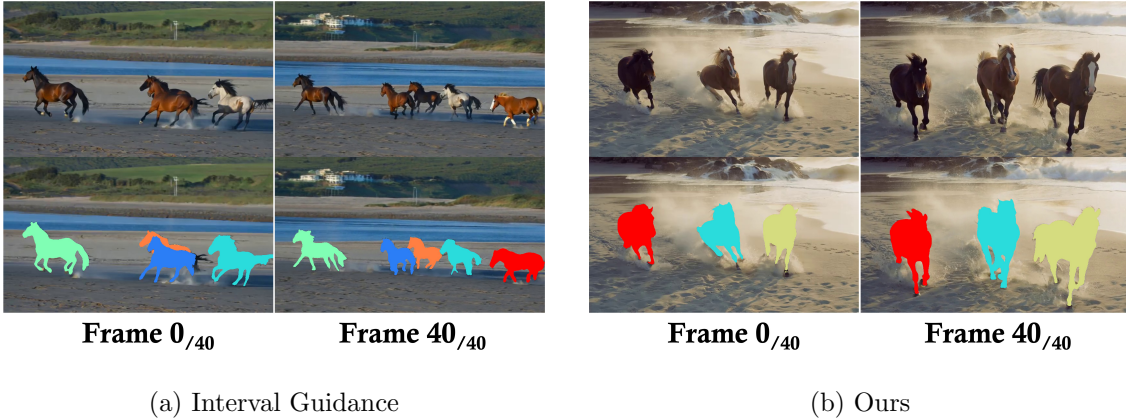


Figure 5: **Qualitative comparison of subject count consistency.** While the Interval Guidance (a) hallucinated an additional horse, our method (b) consistently maintained the requested count of three horses throughout the video.

tion interval too far ($\tau = 0.30$) leads to a performance drop across most metrics. Notably, excessive τ causes a significant degradation in text alignment (X-CLIP drops to 21.9369) and reduces raw pixel-level motion (FLOW decreases from 1.8005 to 1.1102). This indicates that while an appropriate application window is essential for developing structural motion, injecting perturbations over an excessively long schedule corrupts the spatial semantics and ultimately limits overall dynamic fidelity.

4.3 Extension to Object Counting

To demonstrate the versatility of our framework, we investigate whether the semantic perturbation mechanism of MotionCFG can be generalized beyond motion dynamics to other specific attributes, such as numerical quantity. In this experiment, we apply perturbations to the embeddings of quantity-related words instead of motion-related ones. We evaluate the object counting accuracy using the open-world counting framework proposed in CountVid [1], calculating the Mean Absolute Error (MAE) and Root Mean Square Error (RMSE) between the generated videos and ground truth counts.

As summarized in Table 6, MotionCFG demonstrates a clear advantage in numerical alignment compared to the baseline and Interval Guidance (IG). Even with preliminary hyperparameter settings, our method effectively reduces the counting error. For instance, the configuration with $w = 6.0, \tau = 0.2, \sigma_c = 0.5$ achieves an MAE of 2.3952, which is a significant improvement over the baseline MAE of 6.2543. These results suggest that perturbing attribute-specific embeddings during the guidance process can effectively steer the generative model toward precise attribute formation. The variance in performance across different noise scales indicates a need for attribute-specific scheduling. Since different semantic properties likely emerge at different stages of the diffusion process, future work should explore optimal temporal windows and noise intensities tailored to specific attributes beyond motion and quantity.

Table 6: **Object counting performance.** MotionCFG configurations show lower MAE and RMSE.

Method	MAE ↓	RMSE ↓
Baseline ($w = 6.0$)	6.2543	8.3558
IG ($w = 6.0, r = 0.1$)	4.8911	12.0896
Ours ($\tau = 0.2, \sigma_c = 0.1$)	4.1411	11.5924
Ours ($\tau = 0.4, \sigma_c = 0.1$)	4.2056	9.1235
Ours ($\tau = 0.2, \sigma_c = 0.5$)	2.3952	3.6290

5 Conclusion

We introduced MotionCFG, a training-free guidance mechanism designed to rectify the inherent low-motion bias in text-to-video generation. By constructing motion-perturbed negative anchors and steering the latent trajectories away from these degenerate counterparts, MotionCFG selectively sharpens dynamic intent while fundamentally circumventing Content-Motion Drift. This contrastive formulation ensures semantic precision through implicit hard negative mining, effectively refining temporal details without compromising the structural integrity of the scene. When integrated with our piecewise guidance scheduler, MotionCFG consistently improves motion fluidity across diverse T2V frameworks with negligible computational overhead. Furthermore, we demonstrated that this noise-induced contrastive principle serves as a generalized framework capable of steering other elusive, non-linear concepts, such as precise object numerosity. Our findings establish MotionCFG as a robust and versatile tool for high-fidelity, controllable video synthesis, paving the way for more nuanced attribute modulation in diffusion-based generative models.

Limitations and Future Work. Our LLM-based motion token identification introduces a lightweight but non-negligible dependency; exploring more efficient alternatives, such as attention-based saliency, could further streamline the pipeline. More broadly, the core idea of MotionCFG (selectively sharpening specific semantic dimensions via targeted perturbation) is not limited to motion. As we briefly demonstrate with object counting (see Table 6), the same principle can enhance other attributes where standard CFG falls short. Extending this framework to additional semantic axes and developing adaptive scheduling methods that automatically identify the optimal intervention window are promising directions for future work.

References

- [1] Amini-Naieni, N., Zisserman, A.: Open-world object counting in videos. In: Association for Advancement of Artificial Intelligence Conference (AAAI) (2026)
- [2] Baherwani, V., Ren, Y., Shrivastava, A.: Characterizing motion encoding in video diffusion timesteps. arXiv preprint arXiv:2512.22175 (2025)
- [3] Bain, M., Nagrani, A., Varol, G., Zisserman, A.: Frozen in time: A joint video and image encoder for end-to-end retrieval. In: Proceedings of the IEEE/CVF international conference on computer vision. pp. 1728–1738 (2021)
- [4] Blattmann, A., Dockhorn, T., Kulal, S., Mendeleevitch, D., Kilian, M., Lorenz, D., Levi, Y., English, Z., Voleti, V., Letts, A., et al.: Stable video diffusion: Scaling latent video diffusion models to large datasets. arXiv preprint arXiv:2311.15127 (2023)
- [5] Brooks, T., Peebles, B., Holmes, C., DePue, W., Guo, Y., Jing, L., Schnurr, D., Taylor, J., Luhman, T., Luhman, E., et al.: Video generation models as world simulators. OpenAI Blog 1(8), 1 (2024)
- [6] Chen, H., Xia, M., He, Y., Zhang, Y., Cun, X., Yang, S., Xing, J., Liu, Y., Chen, Q., Wang, X., et al.: Videocrafter1: Open diffusion models for high-quality video generation. arXiv preprint arXiv:2310.19512 (2023)

- [7] Choi, J.S., Lee, K., Yu, S., Choi, Y., Shin, J., Lee, K.: Improving motion in image-to-video models via adaptive low-pass guidance. arXiv preprint arXiv:2506.08456 (2026)
- [8] Chung, H., Kim, J., Park, G.Y., Nam, H., Ye, J.C.: CFG++: Manifold-constrained classifier free guidance for diffusion models. The Thirteenth International Conference on Learning Representations (2025)
- [9] Desai, A., Vasconcelos, N.: Improving image synthesis with diffusion-negative sampling. In: European Conference on Computer Vision. pp. 199–214. Springer (2024)
- [10] Hessel, J., Holtzman, A., Forbes, M., Le Bras, R., Choi, Y.: Clipscore: A reference-free evaluation metric for image captioning. In: Proceedings of the 2021 conference on empirical methods in natural language processing. pp. 7514–7528 (2021)
- [11] Ho, J., Jain, A., Abbeel, P.: Denoising diffusion probabilistic models. Advances in neural information processing systems **33**, 6840–6851 (2020)
- [12] Ho, J., Salimans, T.: Classifier-free diffusion guidance. arXiv preprint arXiv:2207.12598 (2022)
- [13] Ho, J., Salimans, T., Gritsenko, A., Chan, W., Norouzi, M., Fleet, D.J.: Video diffusion models. In: Koyejo, S., Mohamed, S., Agarwal, A., Belgrave, D., Cho, K., Oh, A. (eds.) Advances in Neural Information Processing Systems. vol. 35, pp. 8633–8646. Curran Associates, Inc. (2022)
- [14] Jang, S., Ki, T., Jo, J., Yoon, J., Kim, S.Y., Lin, Z., Hwang, S.J.: Frame guidance: Training-free guidance for frame-level control in video diffusion model. In: The Fourteenth International Conference on Learning Representations (2026), <https://openreview.net/forum?id=y39XbEp1vK>
- [15] Kingma, D.P., Welling, M.: Auto-encoding variational bayes. In: Bengio, Y., LeCun, Y. (eds.) 2nd International Conference on Learning Representations, ICLR 2014, Banff, AB, Canada, April 14-16, 2014, Conference Track Proceedings (2014)
- [16] Kirstain, Y., Polyak, A., Singer, U., Matiana, S., Penna, J., Levy, O.: Pick-a-pic: An open dataset of user preferences for text-to-image generation. In: Oh, A., Naumann, T., Globerson, A., Saenko, K., Hardt, M., Levine, S. (eds.) Advances in Neural Information Processing Systems 36: Annual Conference on Neural Information Processing Systems 2023, NeurIPS 2023, New Orleans, LA, USA, December 10 - 16, 2023 (2023)
- [17] Kynkäänniemi, T., Aittala, M., Karras, T., Laine, S., Aila, T., Lehtinen, J.: Applying guidance in a limited interval improves sample and distribution quality in diffusion models. Advances in Neural Information Processing Systems **37**, 122458–122483 (2024)
- [18] Liao, M., Lu, H., Ye, Q., Zuo, W., Wan, F., Wang, T., Zhao, Y., Wang, J., Zhang, X.: Evaluation of text-to-video generation models: A dynamics perspective. In: Globersons, A., Mackey, L., Belgrave, D., Fan, A., Paquet, U., Tomczak, J.M., Zhang, C. (eds.) Advances in Neural Information Processing Systems 38: Annual Conference on Neural Information Processing Systems 2024, NeurIPS 2024, Vancouver, BC, Canada, December 10 - 15, 2024 (2024)

- [19] Lipman, Y., Chen, R.T.Q., Ben-Hamu, H., Nickel, M., Le, M.: Flow matching for generative modeling. In: The Eleventh International Conference on Learning Representations, ICLR 2023, Kigali, Rwanda, May 1-5, 2023 (2023)
- [20] Ma, Y., Xu, G., Sun, X., Yan, M., Zhang, J., Ji, R.: X-CLIP: end-to-end multi-grained contrastive learning for video-text retrieval. In: Magalhães, J., Bimbo, A.D., Satoh, S., Sebe, N., Alameda-Pineda, X., Jin, Q., Oria, V., Toni, L. (eds.) MM '22: The 30th ACM International Conference on Multimedia, Lisboa, Portugal, October 10 - 14, 2022. pp. 638–647. ACM (2022)
- [21] Raffel, C., Shazeer, N., Roberts, A., Lee, K., Narang, S., Matena, M., Zhou, Y., Li, W., Liu, P.J.: Exploring the limits of transfer learning with a unified text-to-text transformer. *J. Mach. Learn. Res.* **21**, 140:1–140:67 (2020)
- [22] Ruan, P., Wang, P., Saxena, D., Cao, J., Shi, Y.: Enhancing motion in text-to-video generation with decomposed encoding and conditioning. *Advances in Neural Information Processing Systems* **37**, 70101–70129 (2024)
- [23] Sadat, S., Buhmann, J., Bradley, D., Hilliges, O., Weber, R.M.: CADs: Unleashing the diversity of diffusion models through condition-annealed sampling. In: The Twelfth International Conference on Learning Representations (2024)
- [24] Shaulov, A., Hazan, I., Wolf, L., Chefer, H.: Flowmo: Variance-based flow guidance for coherent motion in video generation. *arXiv preprint arXiv:2309.03884* (2025)
- [25] Singer, U., Polyak, A., Hayes, T., Yin, X., An, J., Zhang, S., Hu, Q., Yang, H., Ashual, O., Gafni, O., Parikh, D., Gupta, S., Taigman, Y.: Make-a-video: Text-to-video generation without text-video data. In: The Eleventh International Conference on Learning Representations, ICLR 2023, Kigali, Rwanda, May 1-5, 2023 (2023)
- [26] Sun, K., Huang, K., Liu, X., Wu, Y., Xu, Z., Li, Z., Liu, X.: T2v-compbench: A comprehensive benchmark for compositional text-to-video generation. In: *IEEE/CVF Conference on Computer Vision and Pattern Recognition, CVPR 2025, Nashville, TN, USA, June 11-15, 2025*. pp. 8406–8416 (2025)
- [27] Tan, Z., Yang, X., Qin, L., Li, H.: Vidgen-1m: A large-scale dataset for text-to-video generation. *arXiv preprint arXiv:2408.02629* (2024)
- [28] Um, S., Ye, J.C.: Minority-focused text-to-image generation via prompt optimization. In: *Proceedings of the Computer Vision and Pattern Recognition Conference*. pp. 20926–20936 (2025)
- [29] Wan, T., Wang, A., Ai, B., Wen, B., Mao, C., Xie, C.W., Chen, D., Yu, F., Zhao, H., Yang, J., et al.: Wan: Open and advanced large-scale video generative models. *arXiv preprint arXiv:2503.20314* (2025)
- [30] Yang, Z., Teng, J., Zheng, W., Ding, M., Huang, S., Xu, J., Yang, Y., Hong, W., Zhang, X., Feng, G., Yin, D., Zhang, Y., Wang, W., Cheng, Y., Xu, B., Gu, X., Dong, Y., Tang, J.: Cogvideox: Text-to-video diffusion models with an expert transformer. In: *The Thirteenth International Conference on Learning Representations, ICLR 2025, Singapore, April 24-28, 2025* (2025)

A Implementation Details

Hyperparameter Settings.

For MotionCFG, we set the motion guidance scale to $\omega = 6.0$, the scheduling ratio to $\tau \in [0.1, 0.2]$, and the perturbation magnitude to $\sigma_c \in [0.1, 0.5]$. All approaches, including standard CFG, CADs, and Interval Guidance, share the same base guidance scale $\omega_{\text{std}} = 6.0$ for fair comparison.

Delayed Scheduling for CogVideoX. Unlike Wan2.1, CogVideoX exhibits severe artifacts when MotionCFG is applied from the very first denoising step. As shown in Fig. 6, the Tweedie estimate at $t = T$ is dominated by dataset-specific biases (*e.g.*, POND5 watermarks) rather than meaningful semantic structure. Injecting motion perturbation at this stage may amplify these artifacts instead of enhancing dynamics. To address this, we employ a delayed schedule: the first few steps use only standard conditional prediction ($\omega_{\text{std}} = 1.0$) to establish a clean spatial layout, after which MotionCFG is applied over the subsequent interval. This simple modification successfully enhances motion dynamics while preventing early-stage artifact amplification.



Figure 6: **Tweedie estimate of CogVideoX at $t = T$.** The initial clean prediction is dominated by dataset-specific artifacts (*e.g.*, watermarks) rather than semantic content.

Standard Negative Prompts. As baselines for comparison, we employ comprehensive standard negative prompt across all baselines to encourage high-quality generation and heavily penalize low-quality or motionless artifacts. The exact text of the negative prompt used in our evaluations is detailed below:

Standard Negative Prompt

Bright tones, overexposed, static, blurred details, subtitles, style, works, paintings, images, static, overall gray, worst quality, low quality, JPEG compression residue, ugly, incomplete, extra fingers, poorly drawn hands, poorly drawn faces, deformed, disfigured, misshapen limbs, fused fingers, still picture, messy background, three legs, many people in the background, walking backwards

Motion Token Extraction Prompt. We use Qwen2.5-7B-Instruct to automate motion token identification. The input prompt is tokenized with positional indices (*e.g.*, [0]A [1]cat [2]jumps), and the model is instructed to return indices of physical action verbs via few-shot in-context learning. Since modern text encoders (*e.g.*, T5) often split a single word into multiple sub-word tokens, we locate the exact character span of each extracted verb and cross-reference it with the tokenizer’s offset mapping. This yields the precise sub-word token indices, which form our active target set $\mathcal{I}_{\text{motion}}$ for the subsequent semantic perturbation. The full instruction template is shown in the prompt box below.

Instruction Template for Motion Token Identification

```

messages = [
  {"role": "system", "content":
    "You are an AI that identifies ACTION VERBS in a sentence.\n"
    "Given indexed words like [i]word, output ONLY the indices of VERBS\n"
    "that describe physical actions or movements.\n"
    "DO NOT select: nouns, articles (a, an, the), pronouns (it, its, he\n"
    ", she), prepositions (in, on, at), adjectives.\n"
    "If no action verbs exist, return [].\n"
    "Output format: JSON list of indices only, nothing else."
  },
  # Few-shot: Explicit actions
  {"role": "user", "content": "Text: [0]A [1]cat [2]jumps [3]over [4]the\n"
    "[5]fence"},
  {"role": "assistant", "content": "[2]"},

  # Few-shot: Multiple actions
  {"role": "user", "content": "Text: [0]Birds [1]fly [2]and [3]sing [4]in\n"
    "[5]the [6]morning"},
  {"role": "assistant", "content": "[1, 3]"},

  # Few-shot: No actions (nouns only)
  {"role": "user", "content": "Text: [0]A [1]red [2]ball [3]on [4]the [5]\n"
    "table"},
  {"role": "assistant", "content": "[]"},

  # Few-shot: Exclude articles/pronouns
  {"role": "user", "content": "Text: [0]The [1]dog [2]sleeps [3]under [4]\n"
    "a [5]tree"},
  {"role": "assistant", "content": "[2]"},

  {"role": "user", "content": f"Text: {indexed_text}"
}

```

Table 7: Examples from the Gemini-generated evaluation prompts. Motion keywords are in bold.

Category	Text Prompt
Animal	A wild horse galloping through a dusty canyon
Animal	A great white shark swimming aggressively in the deep ocean
Human	A ballet dancer spinning on stage under a spotlight
Human	A chef chopping onions rapidly on a wooden board
Vehicle	A red sports car drifting on a race track with smoke
Vehicle	A space rocket launching into the sky with fire
Nature	A volcano erupting with lava and ash
Physics	An old building collapsing into dust
Abstract	Colorful ink spreading in clear water

Table 8: **Robustness to LLM size for motion token extraction.** The example column shows each model’s extraction for the prompt: “An elephant sprays water with its trunk, a lion sitting nearby.”

Method	Extraction Example	X-CLIP \uparrow	DINO Segm. \uparrow	Info DINO \uparrow	DEVIL \uparrow
Standard CFG	-	22.2369	0.3359	0.0568	0.2785
Qwen2.5-0.5B	“sprays”, “a”, “nearby”	22.5443	0.4114	0.0751	0.3186
Qwen2.5-3B	“sprays”	22.8157	0.4342	0.0751	0.3334
Qwen2.5-7B	“sprays”	22.9234	0.4385	0.0765	0.3391

Gemini-Generated Evaluation Prompts. Existing T2V benchmarks such as T2V-CompBench primarily evaluate spatial composition and attribute binding, often lacking prompts that demand vigorous physical motion. Models can thus achieve high alignment scores with near-static outputs. To address this gap, we curated a motion-intensive prompt set of 100 prompts generated via Gemini, spanning categories including animal behaviors, human actions, vehicle dynamics, and natural phenomena. Each prompt is centered around a distinct action verb describing high-magnitude motion. Representative examples are shown in Table 7.

B Complementary Analyses and Discussions

B.1 Robustness to LLM Size

A potential concern is MotionCFG’s dependency on the accuracy of the LLM used for motion token extraction. To evaluate this, we ablate across the Qwen2.5 family (0.5B–7B) on our full evaluation set. As shown in Table 8, smaller models occasionally misidentify tokens, *e.g.*, Qwen2.5-0.5B with non-verbs such as “a” and “nearby”. Despite such errors, MotionCFG still improves dynamics across all model sizes, with even the 0.5B variant outperforming the baseline (DEVIL: 0.319 vs. 0.279). Performance improves monotonically with LLM accuracy, and Qwen2.5-7B achieves the best overall trade-off, confirming that MotionCFG is robust to imprecise extraction and does not require a large-scale LLM to be effective.

B.2 Computational Overhead

Table 9 reports end-to-end sampling time per video on a single NVIDIA B200 GPU using Wan2.1-T2V-1.3B. Note that MotionCFG adds only ~ 1 second over the baseline, as it requires no architectural modification, *i.e.*, introducing only a lightweight perturbation of text embeddings during the early denoising steps. The LLM inference for motion token extraction is negligible relative to the video diffusion process. Despite this minimal overhead, MotionCFG achieves the highest X-CLIP and DEVIL scores among all methods.

Table 9: **Complexity analysis.** Average end-to-end sampling time (sec/video) on a single B200 GPU with Wan2.1-1.3B. MotionCFG achieves superior temporal dynamics with negligible computational overhead.

Method	Time \downarrow	X-CLIP \uparrow	DEVIL \uparrow
Baseline	76.339	22.2128	0.3069
CADS	76.710	22.7687	0.1973
IG	73.305	23.0677	0.3147
Ours	77.310	23.3881	0.3374

Table 10: **Comparison with FlowMo [24]**. MotionCFG achieves stronger dynamics with less time consumption compared with FlowMo. Time in seconds per video.

Model	Method	Time↓	X-CLIP↑	DINO Segm.↑	Info DINO↑	DEVIL↑
Wan2.1-1.3B	Standard CFG	76.34	22.2369	0.3359	0.0568	0.2785
	FlowMo	106.49	22.4004	0.3558	0.0590	0.3032
	Ours	77.31	22.4008	0.4527	0.0866	0.3572
Wan2.1-14B	Standard CFG	352.52	21.7438	0.2853	0.0430	0.2324
	FlowMo	525.61	22.1167	0.3507	0.0541	0.2822
	Ours	353.41	22.4939	0.4229	0.0733	0.3246

B.3 Failure Cases

While MotionCFG performs reliably under the demonstrated settings ($\sigma_c < 1.0$), extreme perturbation scales can cause generation failures. As shown in Fig. 7, setting $\sigma_c = 3.0$ pushes $\mathbf{c}_{\text{pert},t}$ far from the valid semantic space, and extrapolating away from this out-of-distribution anchor drives the latent trajectory into degenerate regions. This manifests as extreme contrast, loss of fine-grained detail, and large black silhouetted patches. These results confirm that σ_c should be kept moderate (*e.g.*, $\sigma_c < 1.0$) to ensure the perturbed condition remains a meaningful contrastive signal rather than uninformative noise.



Figure 7: **Failure cases under extreme perturbation ($\sigma_c = 3.0$)**. The perturbed condition falls far outside the valid semantic space, causing severe artifacts including over-saturation, loss of spatial detail, and black silhouetting.

C Additional Experiments

C.1 Comparison with Latent Optimization-Based Methods

We compare MotionCFG with FlowMo [24], a concurrent training-free method that enhances motion certainty by minimizing temporal variance through step-wise gradient optimization in the latent space. As shown in Table 10, FlowMo incurs $1.48\times$ the inference time of the baseline on the 14B model due to per-step gradient computation. MotionCFG requires no gradient computation, matching the baseline’s inference cost while consistently outperforming FlowMo in dynamics metrics across both model scales.

C.2 User Study

We conducted a user study comparing MotionCFG against Baseline, CADS, and IG. A total of 32 participants were shown 20 pairs of generated videos and asked to select their preference based on two criteria: *Visual Quality & Text Alignment* (C1), and task-specific performance: either *Motion Dynamics* (C2) or *Counting Accuracy* (C3). All pairs were randomly shuffled to eliminate ordering bias.

Observe in Table 11 that MotionCFG is consistently preferred across all comparisons. For the motion task, our method is favored over the baseline by 93.6% in C2, and maintains a clear lead over CADS and IG in both criteria. For the counting task, MotionCFG is

Table 11: **User study results.** Preference rate (%) of MotionCFG vs. each compared method, judged on visual quality & text alignment (C1) and task-specific performance: motion dynamics (C2) or counting accuracy (C3).

Task	Compared Method	C1: Visual Quality		C2/C3: Task Perf.	
		Ours	Other	Ours	Other
<i>Motion</i>	vs. Baseline	77.42	22.58	93.55	6.45
	vs. CADS	79.35	20.65	89.68	10.32
	vs. IG	85.16	14.84	81.94	18.06
<i>Counting</i>	vs. Baseline	77.42	22.58	69.68	30.32

preferred in both visual quality and counting accuracy over the baseline. These results align with our quantitative findings.

C.3 Video Gallery

Fig. 8 presents animated frame sequences for qualitative comparison. These are best viewed in Adobe Acrobat Reader, which supports embedded animations. The full video results are also available on the project page.

Prompt: *A rabbit ice skates on a frozen lake while a chipmunk builds a snowman*

(a) Baseline

(b) CADS

(c) Interval Guidance

(d) **Ours**

Prompt: *A robot transforming into a car*

(a) Baseline

(b) CADS

(c) Interval Guidance

(d) **Ours**

Figure 8: **Video gallery.** Animated comparisons across methods. MotionCFG generates physically plausible dynamics faithful to the prompt. Best viewed in Adobe Acrobat Reader.